Int. J. Electrochem. Sci., 14 **(2019)** 10642 – 10656, doi: 10.20964/2019.11.40

International Journal of
ELECTROCHEMICAL
SCIENCE
www.electrochemsci.org

Corrosion Resistance and Passivation Behavior of B-containing S31254 Stainless Steel in a low pH medium

Muhammad Saqlain Qurashi[1], *Yishi Cui*[1], *Jian Wang*[1,*], *Nan Dong*[1], *Jingang Bai*[1,2], *Yucheng Wu*[1],*Peide Han*[1,*]

[1] College of Materials Science and Engineering, Taiyuan University of Technology, Taiyuan 030024, China;
[2] State Key Laboratory of Advanced Stainless Steel Materials, Taiyuan 030003, China;
[*]E-mail: jianwang1@126.com, hanpeide@126.com

Received: 14 June 2019 / *Accepted:* 21 August 2019 / *Published:* 7 October 2019

Addition of boron is found to be effective in achieving corrosion resistance and passivation film composition of S31254 stainless steels in a harsh medium that has a low pH. Successfully enhanced corrosion resistance in chloride solutions with different pH and hindrance of the generation of donor densities with semiconducting characteristics are proved by potentiodynamic polarization tests, electrochemical impedance spectroscopy and Mott-Schottky analysis of different parameters. After potentiodynamic polarization, optical microscopic and scanning electron microscopy of the microstructure were analyzed. Results indicate that borated samples become free from pits that serve as initiation sites around the grain boundaries. Passive film characterization using XPS peak deconvoluted spectra and cationic fractions reveal that after boron addition primary elements of the inner and outer passive layers changed significantly. These changes enhanced the compactness, strength and repassivating ability of the film, which is further supported by XPS depth profile studies with respect to atomic and cationic concentrations.

Keywords: Super austenitic Stainless steel; Boron effect; Corrosion; passive film

1. INTRODUCTION

Superaustenitic stainless steels (SASSs) are a kind of highly alloyed stainless steel in which Cr, Mo and Ni are present in large quantity. Because of this alloy combination, these steels possess excellent electrochemical and mechanical properties. These characteristics of SASS make it possible for it to be widely used in desalination and pulp bleaching systems, heat exchangers, marine engineering, chemical processing, flue gas desulfurizing units, waste incineration plants and nuclear industries [1-3]. SASS S31254 is one of these kinds of steels; its chemical composition has a high amount of chromium (19.5% to 20.5%), molybdenum (6-6.5%), and nickel (18 %), and thus, it exhibits excellent corrosion resistance and superior mechanical properties in harsh media and severe environments [4, 5]. S31254 is a high

strength stainless steel that contains molybdenum (6% Mo) and possesses a higher concentration of alloying elements as compared to conventional stainless steels such as 304, 306 and 306L. Because of the synergistic action of its alloying elements, S31254 shows excellent corrosion resistance in chloride solution [6]. For superaustenitic stainless steel, the higher amounts of chromium and molybdenum inhibit the promotion of macro-segregation of the elements to the interdendritic regions (IDRs) in castings during the solidification process [7]. However, high content of Cr and Mo results into precipitates, sigma phase, and chi phase, which seriously reduce corrosion resistance [8, 9].

Synergy of alloying elements in a passive film has a great effect on the stability and protectiveness of the passive film. If the inner and outer layers are enriched with molybdenum along with chromium as in the S31254-6% Mo alloy, this synergetic effect hinders the dissolution of a passive film comprised of chromium oxides [10]. There are many studies regarding S31254 in acidic media but there are fewer studies regarding the passivation behavior. Liu et al. [11] investigated the passivation behavior of S31254 in low pH (0.8 and 5) and determined the primary constituents of the outermost ($Cr(OH)_3$ and iron oxides) and innermost (Cr_2O_3) layers of the passive film. He also stated that molybdenum oxides are the main contents of the film; specifically, Mo(VI) is in the outer rich layer, and Mo(IV) is in the inner rich layer. Molybdenum species in the inner layers become an obstacle that prevents further dissolution of partial cations through the passive film. The Mo(IV) species in the inner layer act as a barrier that prevents the outward dissolution of partial cations through the passive film. It can be concluded that the main role of Mo is similar to that of Cr in the passivation of steel.

In different studies, attempts have been made to enhance the corrosion resistance and passive film stability via the addition of different alloy elements in stainless steel. In commercial stainless steels, a common method to enhance corrosion resistance and passivity is the addition of Cr, Mo, and Ni [12]. This research work is focused on the effects of added boron, and specifically how it impacts on the passivation behavior of S31254. The addition of boron in this metal has not yet been studied in terms of passivation and corrosion resistance. Boron atoms segregate around the grain boundaries and result in a lowering of the grain boundary energy and inhibition of the nucleation of the second phase, which result into corrosion. This effect can be achieved with the use of a very small amount of B, (parts per million), and this has significant impacts on the production process of steels [13, 9]. Tieming guo et al. [14] reported that the addition of boron lowers the reactivation rate and corrosion rate, and improves intergranular corrosion and the repair capacity of passive films. Our group has studied how boron reduces the sigma phases and enhances the synergy of alloying elements, which decrease the inclusions and increase the microstructural characteristics [1, 8]. It happens due to the segregation of boron atoms at the grain boundaries in the form of the B-2p orbital and enhances the grain boundary strength by combining with the non-bonding states of the iron atoms [15]. F.P.A Robinson and W. G. Scurr [16] stated that adding boron (in ppm) retards and dissolves $Cr_{23}C_6$ precipitates and thus, boron had marked beneficial effects on intergranular corrosion resistance of steel; also, pitting resistance improves. This chromium dissolution results in free Cr in the austenite matrix, and this free Cr soon reacts with other elements like with B and O to make borides $(Cr,Fe)_2B$ and oxides (Cr_2O_3, $Cr(OH)_3$), which are good for self-healing or repassivating ability in stainless steel [17].

In this study, the effect of the presence of boron (in parts per million) on the passivation behavior of S31254 is studied in a harsh medium that has low pH, and the effects are explained after conducting

the electrochemical experiments. Finally, quantitative and qualitative measurements were done for chemical characterization of the passive film using XPS depth profile studies with different parameters.

2. EXPERIMENTAL METHODOLOGY

2.1 Material and solution

Table 1 shows the chemical composition of S31254 superaustenitic stainless steel both with and without added boron, according to the ASTM A312 composition standard. The steels were smelted in a vacuum induction furnace at Taiyuan Iron and Steel Group Co., Ltd (TISCO). Hot rolling of the ingots was done at 1250℃ until a thickness of 12mm was obtained. Then from those plates, sample specimens were cut to 15×15×3 mm^3 using a CNC cutting machine. Samples were quenched after homogenization at 1220℃ for 5 h.

Table 1. Chemical composition (wt%) of the samples of the both samples.

Grade	C	Si	Mn	P	S	Cr	Ni	Mo	Cu	N	B
S31254-0B	0.010	0.61	0.430	0.024	0.001	20.18	18.00	6.00	0.69	0.193	0.000
S31254-40B	0.014	0.62	0.440	0.014	0.006	20.15	18.11	6.12	0.72	0.200	0.004

After embedded in mounting press in a hard thermosetting epoxy resin each sample was mechanically ground with sand-paper from grit 120 to 2500, and then polished until it had a mirror-like surface. Before further experiments, all of the samples were cleaned ultrasonically in ethanol and distilled water. For electrochemical experiments, 3.5% NaCl solutions with different pH values were prepared, HCl and NaOH were used to adjust the pH. For metallographic surface analysis and passivation purposes, a different solution was used; the pH of this solution was -0.3. All of the experiments were conducted at room temperature, and atmospheric pressure. Passivation was done for up to 20 h.

2.2 Experimental technique

After sample preparation and solution making potentiodynamic polarization was carried out first . 3.5% NaCl solutions with different pH values were used as an electrolyte in a three-electrode corrosion cell. A saturated calomel electrode (SCE) was used as the reference electrode, platinum foil was used the counter electrode, and the sample was used as the working electrode with an exposure area of 1cm^2. Polarization curves were recorded at 0.5mVs^{-1} in acidic solution after open circuit potential was stabilized for 30 min. Each experiment was performed three times at room temperature and under atmospheric pressure. After polarization, electrochemical impedance spectroscopy was conducted in the same solution followed by the open circuit potential (OCP) condition under which a passive film was developed on the samples [18-19]. After EIS, Mott-Shottky analysis was done in the solution of the same electrolyte with a different potential for examining the semiconducting properties of the passive film, because passivation properties of stainless steel are associated with the semiconducting properties [20].

After electrochemical experiments, surface analysis was conducted using an optical microscope and scanning electron microscope, and X-ray photoelectron spectroscopic measurements were recorded after 20 h passivation. Then, XPS curve deconvoluted spectra were recorded using the commercial software package XPSPEAK4.1, which was adjusted on the Shirley background subtraction and Gaussian-Lorentzian tail function, to achieve better spectral fitting. After peak deconvolution for each specimen, cationic and atomic fractions were determined, and a comparison of each was explained using XPS depth profile studies.

3. RESULTS AND DISCUSSIONS

3.1 Potentiodynamic polarization

Figure 1 shows the polarization of behavior of steel under acidic conditions (3.5% chloride solutions at different pH values) and is compared with borated and nonborated stainless steel samples.

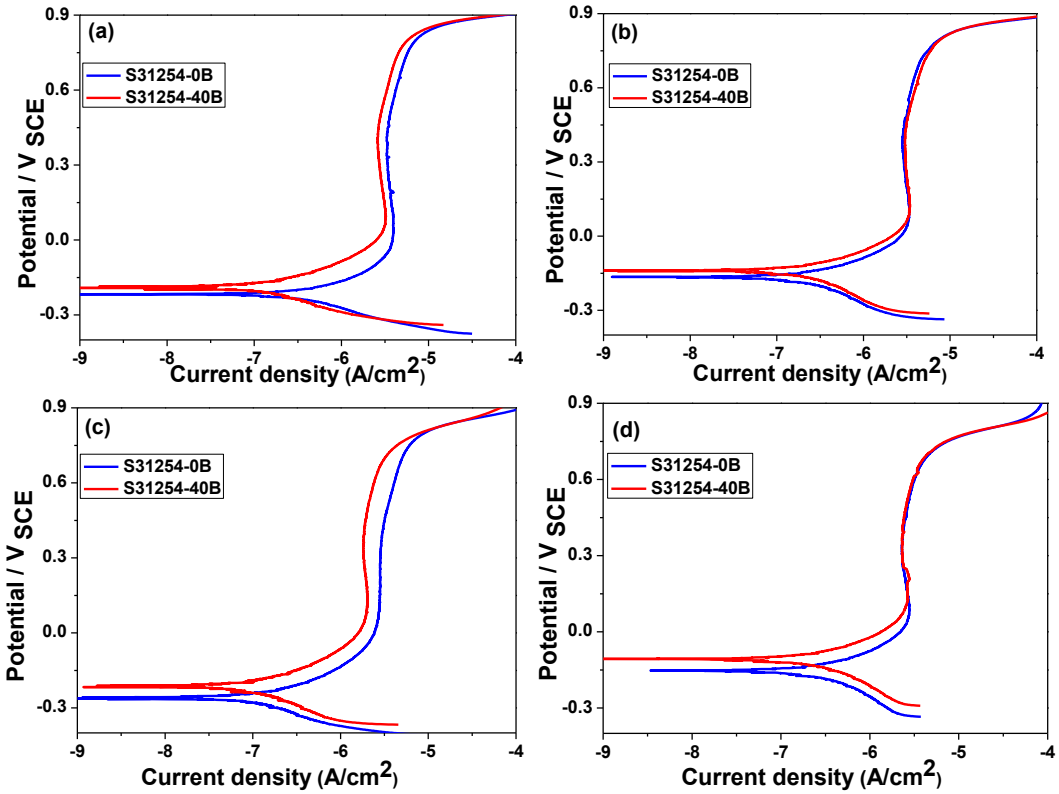

Figure 1. Potentiodynamic polarization curve of S31254 stainless steel in 3.5% NaCl solution (a) pH 0.4 (b) pH 0.9 (c) pH 2.0 (d) pH 2.5

Effects of acidity or pH are well know; specifically, it is known how chloride and sulfide ions accelerate corrosion. A harsh acidic environment or chloride environment can easily deteriorate or perforate the surface of steel [21] and cause the nucleation of pits that serve as initiation sites. It can be seen that both types of specimens have almost the same trends. The corrosion rate and corrosion current densities (*Icorr*) are enhanced in nonborated samples, as seen in Table 2. Corrosion current densities (*Icorr*) reflect the dissolution rate of a passive film during the passivating process. Thus, a higher passive

current density leads to a higher dissolution rate in the passive film, and this indicates the protective ability of the passive film was low [22]. Moreover, the potential also shifted in the positive direction in each of the solutions that had different pH values. From these observations, it can be concluded that adding boron makes the passive film stable.

Table 2. Data fitted for polarization curves

Sample	*Ecorr* (mV)	*Icorr* (A cm^{-2})	*Corr-Rate* (mmPY)
S31254-0B-0.4pH	-0.217	5.937E-07	1.396E-02
S31254-40B-0.4pH	-0.187	9.727E-08	2.288E-03
S31254-0B-0.9pH	-0.165	3.65E-07	8.591E-03
S31254-40B-0.9pH	-0.139	3.389E-07	7.972E-03
S31254-0B-2.0pH	-0.262	4.066E-07	9.566E-03
S31254-40B-2.0pH	-0.212	1.291E-07	3.038E-03
S31254-0B-2.5pH	-0.152	3.792E-07	8.921E-03
S31254-40B-2.5pH	-0.106	1.132E-07	2.663E-03

These observations regarding increased corrosion resistance due to boron are in good concordance with many previous studies on different Fe-Cr alloys, because boron slows the reactivation rate and improves passivating ability of the oxide film [14, 16]. In the latest research, scientists have found a boron positive effect on the hindrance of pitting corrosion and intergranular corrosion, because boron eliminates the precipitation and decreases the corrosion depleted regions near the grain boundaries [23]. It has been found that another reason is that boron dissolves the metal carbides such as chromium carbides and enhances the boron carbides, and this results in hindering corrosion [24].

3.2 Electrochemical impedance spectroscopy

Figure 2 shows Nyquist (a) and Bode plots (b, c) for data recorded after the open circuit potential stabilized in 30 min in chloride solutions with different pH values. The Nyquist plot in Figure 2(a) exhibits an arc of a depressed semicircle; the arc of the semicircle in a Nyquist plot indicates the corrosion resistance, which is relative to the diameter [25, 26]. In the case of the borated sample, the diameter of the arc of the capacitive semicircle is increased, and this indicates that the sample has a stable passive film and less corrosion. Figure 2(b, c) shows a Bode plot comparison; the sample with boron has a higher phase degree, suggests that this sample has a more condensed and intact passive film [27]. Therefore, the results of these EIS experiments indicate that adding boron is a promising approach because it leads to enhanced contamination corrosion resistance and passive film stability.

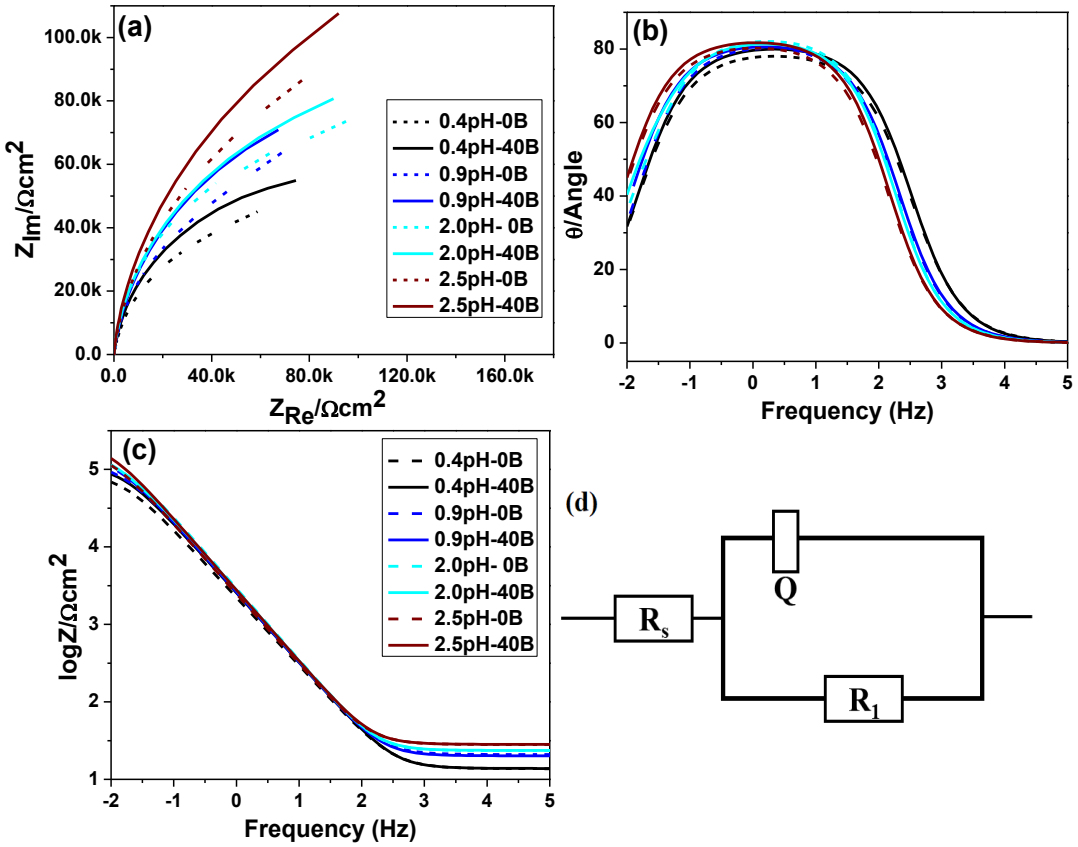

Figure 2. Electrochemical impedance spectroscopy of the S31254 stainless steel in 3.5% NaCl solution of different pH. (a) Nyquist plot (b,c) bode plots, (d) electrical equivalent circuit of the sample/solution interface. Dashed lines are representing S31254-0B and straight lines S31254-40B

Table 3. EIS Nyquist plot data fitting

Sample	R_s (Ω cm^2)	Q ($\Omega^{-1}s^{-n}cm^2$)	n	R_1 (Ω cm^2)
S31254-0B-0.4pH	13.72	8.832E-5	0.882	9.074E+4
S31254-40B-0.4pH	13.81	7.419E-5	0.902	1.310E+5
S31254-0B-0.9pH	20.88	7.298E-5	0.906	1.211E+5
S31254-40B-0.9pH	20.11	7.160E-5	0.910	1.498E+5
S31254-0B-2.0pH	23.45	6.303E-5	0.924	1.439E+5
S31254-40B-2.0pH	23.55	6.741E-5	0.915	1.619E+5
S31254-0B-2.5pH	28.08	7.596E-5	0.907	1.828E+5
S31254-40B-2.5pH	28.25	6.588E-5	0.922	2.235E+5

Figure 2(d) shows an electrical equivalent circuit that represents the electro-chemical connection between the interface and the specimen described by the Nyquist plot. This electrical model is used for fitting the data of the Nyquist plot. This model is classically used to describe electrochemical reactions at an electrode/electrolyte interface of a passive system when an intact layer of passive film is considered [28]. The electrochemical impedance parameters obtained from fitting the Nyquist plot data is given in

the Table 3. Here R_s represents the solution resistance, R_1 represent the charge-transfer resistance, and Q is the double charge layer capacitance [27]. As seen in Table 3, the boron-contaminated samples have higher R_1 at each pH. The higher R_1 of borated samples is the proof of less decomposition or dissolution of the passive film. This is also consistent with the latest research regarding the effect of boron in different media; furthermore this higher resistance to corrosion is because of the thickness of oxide film and lower dissolution of the oxide film [14, 24].

3.3 Mott-schottky analysis

Mott-Schottky measurements are conducted to examine the semiconducting characteristics of a passive film because the passivation properties of stainless steel are also associated with the semiconducting characteristics, including the carrier densities and diffusion coefficient [29]. Here, the test was performed in the same chloride solution (pH 2) but different voltages were used. All of the curves are positively sloped and exhibit the characteristics of n-type semiconductors. However, with an increase in voltage, the slope of the curve becomes steeper. N-type semiconducting characteristics are recorded as donor densities. It is probable that the n-type oxide films Fe_2O_3 and $Fe(OH)_3$ formed on the sample [30]. The plots show a linear region over a potential range. This linear region is due to changes in the width of the space layer of the oxide film on the specimen with a given potential (v) according to the expression

$$\frac{1}{C^2} = \frac{2}{\varepsilon\varepsilon_o e N_d A^2}\left(E - E_{jb} - {}^{kT}/_{e}\right) \quad \text{N-type}$$

where E is the applied potential (V_{SCE}), E_{fb} is the flat band potential (V_{SCE}), e_o is the permittivity of free space (F cm^{-1}). N_d is the donor density (cm^{-3}), N_a is the accept density (cm^{-3}), A is the surface area of the sample (cm^2), k is the Boltzmann constant (1.38 *10^{-23} J/K), T is the absolute temperature and e is the charge of the electron (1.6*10^{-19} C) [31]. The donor density, N_d of the outer iron oxide layer exposed to the electrolyte, can be determined from the curve of this plot. N_d is inversely related to the plots of C_{SC}^{-2} versus E, which should be linear with a positive slope.

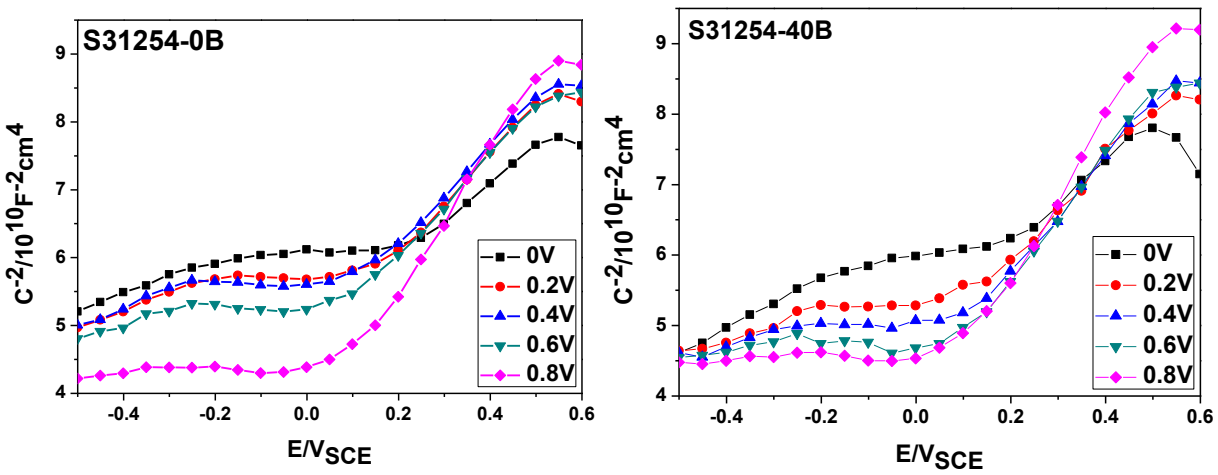

Figure 3. Mott-schottky analysis of S31254 stainless steel at different voltage in chloride solution of 2pH

The densities of the passive film can be attributed to the different voltages and to the boron content in the samples. Because higher donor densities may be associated with more disordered structures of the passive films, lower donor densities may correspond to a more stable and sound passive films [32, 33].

Table 4 is showing the donor densities, the densities of the B contained sample is lower comparatively. Therefore, S31254 with boron has non-disordered non-porous passive film.

Table 4. Fitted data of Mott-Schottky measurements

Potential (V)	**S312542-0B ND (10^{22} at cm^3)**	**S31254-40B ND (10^{22} at cm^3)**
0	1.147E+22	9.198E+21
0.2	8.180E+21	7.723E+21
0.4	7.439E+21	6.580E+21
0.6	6.885E+21	3.271E+21
0.8	5.594E+21	5.249E+21

3.4 Surface Morphology

3.4.1 Metallographic Structures

A surface analysis study was conducted after potentiodynamic polarization in the solution with a pH of -3 at room temperature. Here, the pitting potential of the borated sample (0.94822 mV) is higher than that of the nonborated sample (0.91407mV), and this is consistent with scanning electron microscopic structures (shown in Figure 4). There the trend of the curve is different from the curves obtained in higher pH solution (Figure 1). As observed in the comparison of scanning electron microstructures shown in Fig 4 (b, c) pits and grain boundary erosion damage are nucleated around the three points of the grain boundaries of nonborated samples, but the borated samples (d, e) remained safe from this grain boundary erosion damage that can lead to pit initiation. O'Laoire et al. [34] found almost the same pits around the grain boundaries during acid treatment. Many authors have stated that boron favorably increases corrosion resistance and enhances the passivating ability of the steel [14, 16]. This indicates that boron has strong resistance to intergranular corrosion under the same corrosion conditions. Therefore, it can be concluded that adding boron significantly reduces the number and size of inclusions and hinders perforation. These results are consistent with the electrochemical measurements presented in Figure 1 and 2. On the basis these outcomes it is suggested that boron can be used to improve corrosion resistance of SASS.

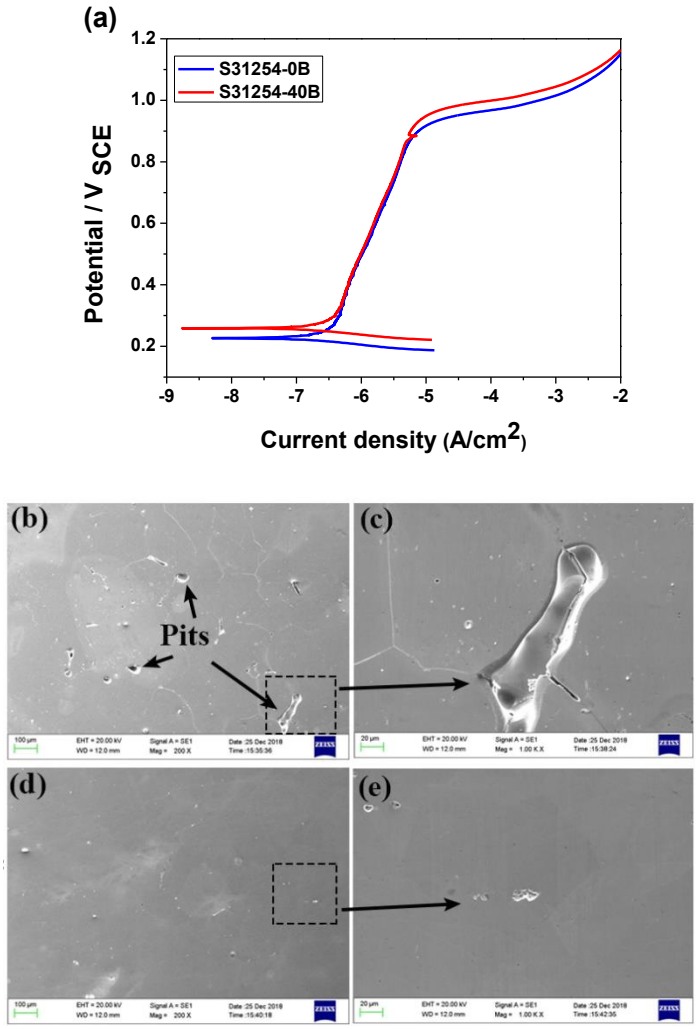

Figure 4. Scanning electron microscopic structures of S31254 stainless steel after potentiodynamic polarization (a) polarization curve (b, c) S31254-0B, (d, e) S31254-40B

3.4.2 XPS measurements

The chemical composition of the passive film that forms in a severe harsh environment, is investigated using XPS. Spectra deconvolution of the primary elements (Cr, Fe, Mo, Ni, and O) of S31254 passive film are presented in Figure 6 according to their binding energies. Figure 6(a) is the deconvolution of the sample without boron and Figure 6(b) is that of the sample with boron. The spectrum of each element is split into subspecies such as in oxides with respect to respective intensities and binding energies. The strongest spectra of chromium $2p_{3/2}$ is split into Cr_{met} (574.1 eV), Cr_2O_3 (576.3 eV), and $Cr(OH)_3$ (577.3eV), and that of iron $2p_{3/2}$ is split into Fe_{met} (707.0 eV), bivalent (Fe(II) 709.4 eV), and trivalent (Fe(III) 711.0 eV) species as recorded in each sample in Figure 6. The exception is sample (b) in Figure 6, in which iron is not split into its species. Molybdenum 3d has relatively low intensities compared to chromium in two kinds of energy levels Mo $3d_{3/2}$ and $3d_{5/2}$. The six overlapping constituent peaks indicate the metallic (Mo_{met} 227.4&230.9 eV) four-valence (Mo^{4+} 230.2&233.4 eV) and six-valence (Mo^{6+} 232.2&235.1eV) species. For the nickel Ni $2p_{3/2}$ spectra, there are also three different signals that were detected: Ni_{met} (852.8eV), NiO (854.3eV) and $Ni(OH)_2$ (855.6eV).

From the peak analysis, it is clear that chromium oxides are abundant in the outermost layer of the passive film of the borated sample, whereas the quantity of iron oxides is less. In recent studies, it has been found that after the addition of boron in S31254 stainless steel, Cr oxides increased significantly in the passive film, and these diffused from the austenitic matrix into the passive layers. This enrichment of Cr species in the outer and inner oxide layers is the strong evidence in favor of adding boron [23, 35]. The percentage of nickel and molybdenum species slightly decreased in the outermost layer of passive film in the borated sample. In Figure 5, a clear difference between the optical microstructures of the borated and nonborated samples is also observed and this reinforces further investigation regarding the surface study. In Figure 5(b) it is found that the top surface does not have pits or pits initiation sites and grain damage/deterioration because boron causes metal carbides to dissolve into the austenitic matrix and lowers the grain boundary energies. These factors stop the pitting phenomenon. In contrast, the top surface of the sample without boron (Fig. 5(a)), shows grain deterioration that leads to pit initiation because of higher the reactivation rate and grain boundary energy [14, 16].

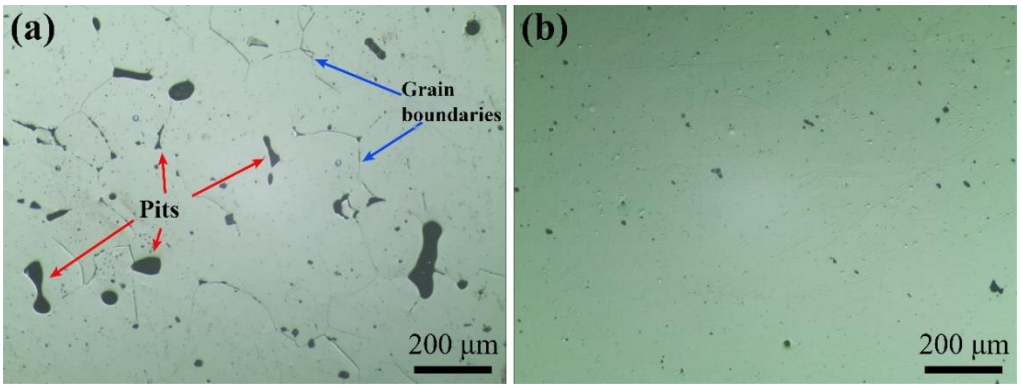

Figure 5. Optical microstructures of S31254 stainless steel (a) S31254-0B (b) S31254-40B

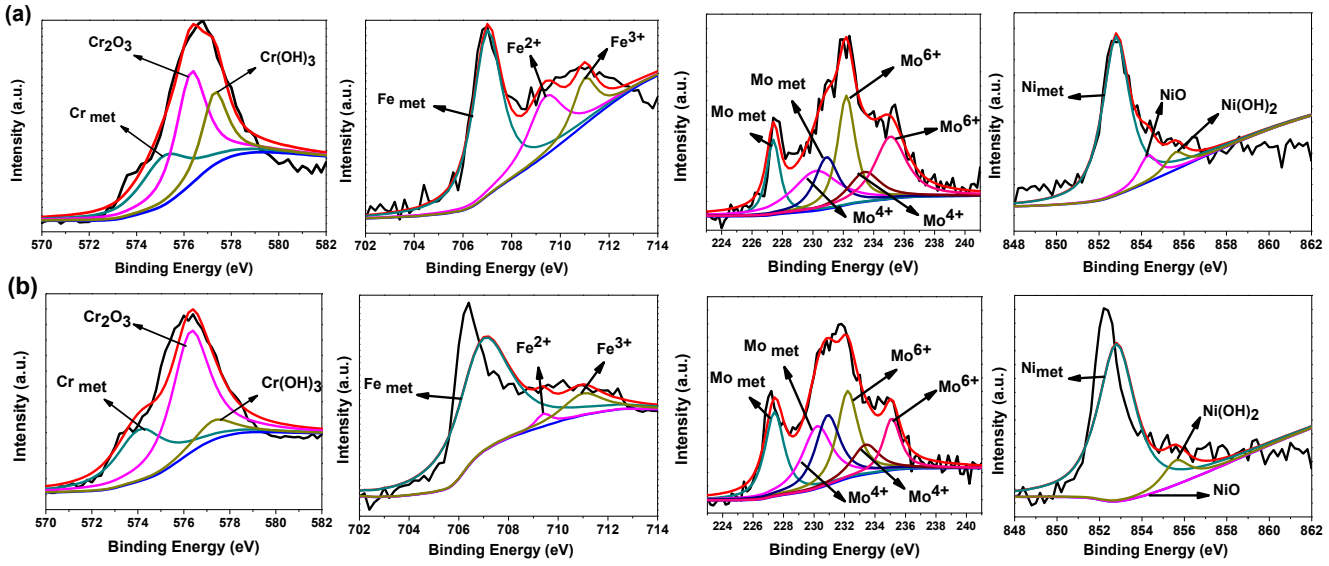

Figure 6. XPS spectra de-convolution of S31254 stainless steel surface. (a) S31254-0B (b) S31254-40B

To gain better and clear understanding of the relationship among these elements, cationic fractioning was conducted, through which it is possible to determine clear chemical composition percentages or effects of passivation time with respect to boron addition. From XPS peaks, apparent conclusions could be drawn from the peak heights but it is necessary to link these conclusions with cationic fractions. Figure 7 depicts the cationic fractions of chromium, iron, molybdenum, and nickel oxides in the outermost layer of the passive film. This was determined using the formula given below [36]

$$C_x = \frac{I_x/S_x}{\sum I_i/S_i}$$

Here cationic fractions and peak intensity are C_x and I_x respectively. The intensity I_x is associated with the peak areas calculated using XPSPEAK 4.1 software. S_x represents the sensitivity factor, which depends on the XPS instrument. This is a quantitative study, and is related to the peaks of each element in the outermost layer of passive film. Loable et al [37] reported that Cr species are basic and the most important for compactness and repassivating ability of a passive film.

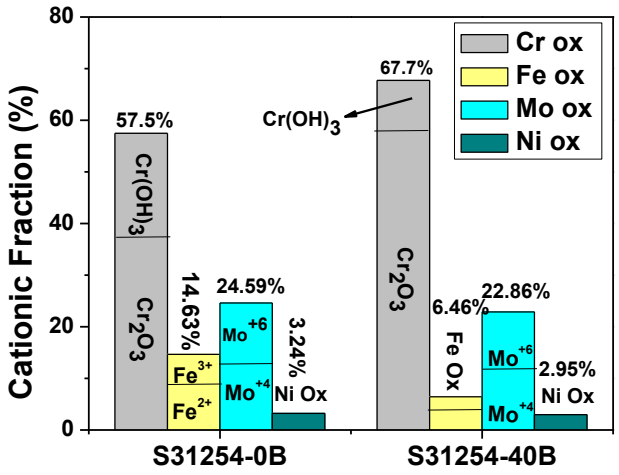

Figure 7. XPS Cationic fraction (C_x) of S31254 with and without Boron after 20h passivation

4.3 XPS depth profiles

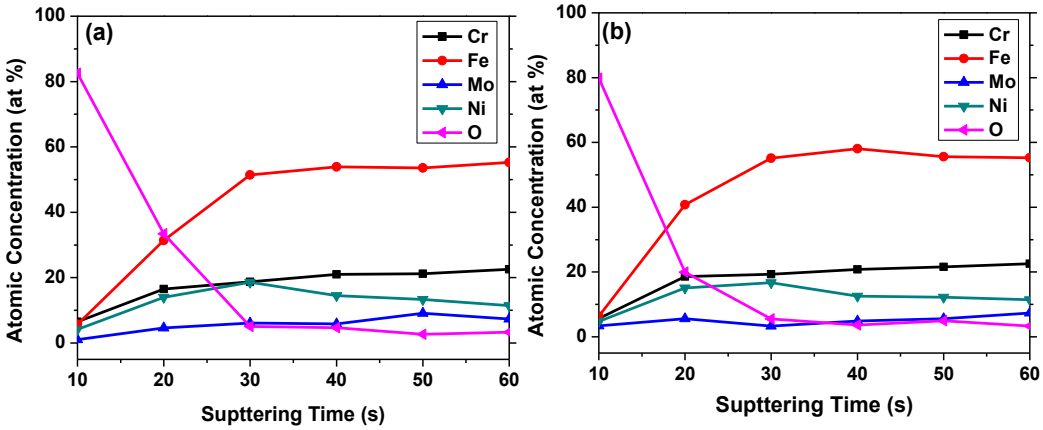

Figure 8. XPS sputtering depth profiles of the distribution of the alloyed elements of S31254 stainless steel (a) S31254-0B (b) S31254-40B

In XPS depth profiles detailed distributions of the elements of the passive film are investigated. Results are shown in Figure 8. Table 5 shows a comparison of the concentration of elements after 10 second sputtering, and this data corresponds to Figure 8. The data show that during the initial stage of the sputtering period, the concentration of Cr is less and that of Fe is higher in the passive film of the sample with boron as compared to the corresponding concentration in the sample without boron.

Table 5. Concentration of the elements during the initial stage of the sputtering (10s)

Sample	Cr (at. %)	Fe (at. %)	Mo (at. %)	Ni (at. %)	O (at. %)
S31254-0B	6.42	5.67	2.087	4.154	81.65
S31254-40B	5.71	6.44	3.41	4.78	80.56

As seen in Figure 8, after a sputtering time 30s, the concentration of elements becomes constant and approaches the alloying ratio. Therefore, it can be speculated that there exists an interface between passive film and metal substrate. Moreover, the depth profile of the Ni concentration is high up to 30s of the sputtering time, and this indicates that Ni is the primarily element that accumulates underneath the passive film/metal substrate interface. A relatively lower concentration of Cr in the initial stages (Table 5) of the sputtering indicates that at this stage, Cr (as opposed to Ni) dominates the competitive oxidation above the interface

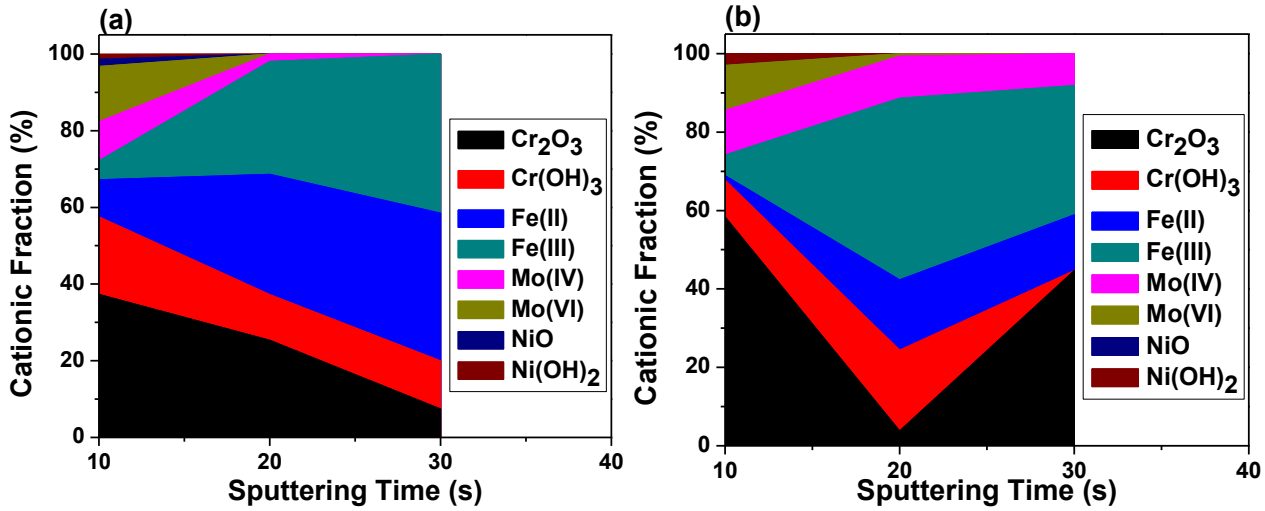

Figure 9. XPS sputtering depth profiles of the oxides in the passive film of S31254 stainless steel. (a) S31254-0B (b) S31254-40B

Figure 9 depicts the oxide variations in the passive film for the 30-second sputtering time. In this cationic fraction comparison, the outer layer of the borated sample has lot of Cr_2O_3 and less iron oxides but the nonborated sample has less Cr_2O_3 and more iron oxides; this clearly shows that the boron-contaminated sample has a strong and protective outer layer of passive film as compared to the nonborated sample. The inner layer of the borated sample is enriched with Cr_2O_3 and impoverished with iron oxides; these observation clearly indicate that the inner layer is also strong and protective. Compared to other oxides, NiO was observed in the passive film in a very much lower quantity. Studies report that

NiO mostly dissolves in the austenite matrix and partly accumulates underneath the passive layers because transfer rate of nickel is lower than that of other elements in the film [38]. Moreover, the inner layer is also enriched with Mo, and it is proposed that Mo mitigates the breakdown of passive film and to promotes passive film repair [39, 10].

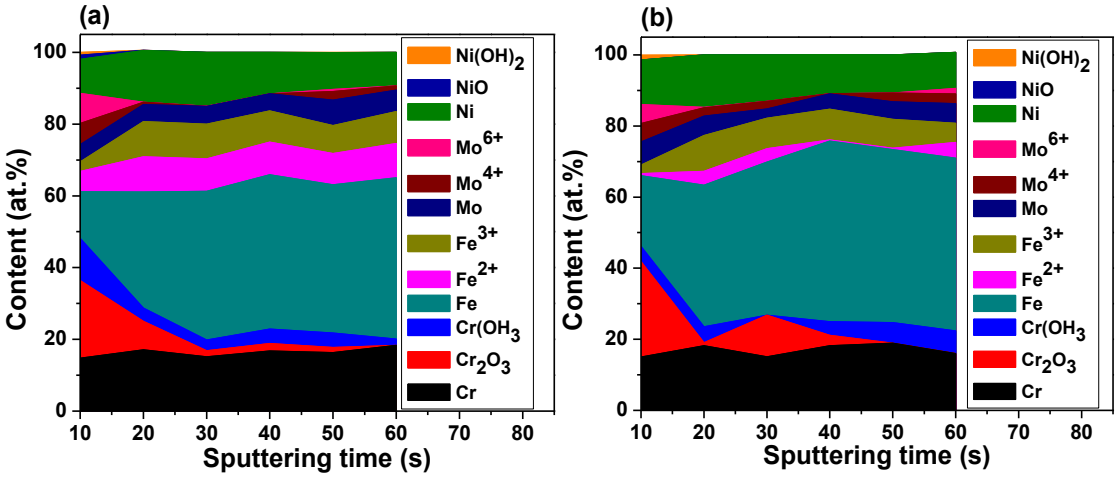

Figure 10. Fraction of the species in the passive film on S31254 stainless steel. (a) S31254-0B (b) S31254-40B

Figure 10 represents the fractions of species with respect to the outer, inner and metal substrate. Up to the 30 second sputtering time period, the distributions of alloying elements and their species vary a lot, and just above the 30 second sputtering fraction, they become nearly constant. Here, if we compare both kinds of samples, there is a higher fraction of Cr_2O_3 in the borated sample in both the outer layer and inner layer. There is also a higher concentration of Mo species in the, and this is promising [39]. Therefore, it can be speculated that boron reinforces those elements in the passive layer, and this is responsible for protecting or stabilizing the passive film of S31254.

5. CONCLUSION

Influences of boron in S31254 were studied in chloride solution using electrochemical tests. After that, quantitative and qualitative evaluations of the passive film for both kinds of samples were conducted. The results are as follows:

1. From electrochemical potentiodynamic polarization, electrochemical impedance spectroscopy and Mott-Schottky analysis, it was revealed that, boron hinders the corrosion rate and enhances the passive strength.
2. Microstructural analyses (SEM and OM) show that boron-contaminated samples have almost a negligible amount of inclusions around the boundaries and pit initiation sites.
3. In XPS peaks and the cationic fraction, it is clear that the sample that contains boron is good. In the atomic distribution, elements vary up to the 30 second sputtering period. After that the element and compound compositions become almost constant. This means that there is an interface

between the film and metal. It is speculated that from 10 s to 30 s of sputtering time, the film has an outer layer and inner layer.

4. From a comparison of the cationic distributions, it is concluded that the borated sample has a compact and dense passive film. The outer layer is enriched with Cr_2O_3, and the inner layer has Cr_2O_3 and Mo(IV) as the primary constituents. From the fractions of all of the elements in the passive film, the borated samples are found with higher percentage of chromium oxides.

ACKNOWLEDGEMENTS
The present work was financially supported by National Natural Science Foundation of China (Grant No. U1860204, No 51871159), the Natural Science Foundation of Shanxi Province (Grant No. 201801D221125, No. 201601D202033, No. 201601D202034) and Innovation Project for Graduate Education of Shanxi province (Grant No. 2018SY012).

References

1. K. H. Lo, C. H. Shek, J. K. L. Lai, *Mater. Sci. Eng. R-Rep, 65*(2009)39
2. H. Li, S.Yang, S. Zhang, B. Zhang, Z. Jiang, H. Feng, J. Li, *Mater. Des*.118(2017)207
3. J. Bai, Y. Cui, J. Wang, N. Dong, M. S. Qurashi, H. Wei, P. Han, *Metals, 8(2018)497.*
4. S. Zhang, Z. Jiang, H. Li, H. Feng, & B. Zhang, *J. Alloy Compd.*, 695(2017)3083
5. H. Li, B. Zhang, Z. Jiang, S. Zhang, H. Feng, P. Han, Q. Lin., *J. Alloy Compd., 686(2016)326*
6. E. A. Abd El Meguid, & A. A. Abd El Latif, *Corros. Sci., 49(2007)263*
7. Y. Hao, W. Liu, J. Li, B. Nie, W. Zhang, & Z. Liu, *Mater. Sci. Eng. A, 736(2018)258*
8. J. Bai, Y. Cui, J. Wang, N. Dong, M. S. Qurashi, H. Wei, P. Han, *J. Iron Steel Res. Int.,* (2018)
9. S. Zhang, Z. Jiang, H. Li, B. Zhang, S. Fan, Z. Li, H. Zhu., *Mater. Charact., 137(2018)244*
10. L. Jinlong, L. Tongxiang, & W. Chen, *Mater. Lett., 171(2016)38*
11. C. T. Liu, & J. K. Wu, *Corros. Sci., 49(2007)2198*
12. D. A. Moreno, B. Molina., C. Ranninger, F. Montero, & J. Izquierdo, *CORROSION., 60(2004)573*
13. J. Takahashi, K. Ishikawa, K. Kawakami, M. Fujioka, & N. Kubota, *Acta Mater., 133(2017)41*
14. T. M. Guo, D. C. Zhang, Z. Hui, C. S. Han, & L. M. Zhao, *Adv. Mater. Res., 415(2011)800*
15. M. Hashimoto, Y. Ishida, S. Wakayama, R. Yamamoto, M. Doyama, & T. Fujiwara, *Acta Mater., 32(1984)13*
16. F.P.A. Robinson, & W.G. Scurr, *Corosion*, 33(1977)408
17. P. Rajesh Kannan, V. Muthupandi, K. Devakumaran, C. Sridivya, & E. Arthi,. *Mater. Chem. Phys., 207(2018)203*
18. M. BenSalah, R. Sabot, E. Triki, L. Dhouibi, P. Refait, & M. Jeannin, *Corros. Sci., 86(2014)61*
19. D. Xia, S. Song, R. Zhu, Y. Behnamian, C. Shen, J. Wang, S. Klimas, *Electrochim. Acta, 111(2013)510*
20. D. D. Macdonald, *Electrochim. Acta, 56(2011)1761*
21. V.B. Singh, & M. Ray, *Int. J. Electrochem. Sci.,* 2(2007)329
22. H. Luo, X. Wang, C. Dong, K. Xiao, & X. Li, *Corros. Sci., 124(2017)178*
23. J. Wang, Y. Cui, J. Bai, N. Dong, Y. Liu, C. Zhang, P. Han, *Mater.Lett.*, 252(2019)60
24. H-R. Marco A.L., L-C. Dionision A., L. Diego., M-C, Gabriela., and B-G. Yeneth., Metals, 9(2019)307
25. D. P. Le, W. S. Ji, J. G. Kim, K. J. Jeong, & S. H. Lee, *Corros. Sci., 50(2008)1195*
26. G. Zou, W. Shi, S. Xiang, X. Ji, G. Ma, & R. G. Ballinger, *RSC Advances, 8(2018)2811*
27. J. Wang, Y. Liu, Y. Qiao, Y. Hu, Y. Cui, P. Han, *Int. J. Electrochem. Sci.,* 12 (2017)6492
28. Z. Cui, L. Wang, H. Ni, W. Hao, C. Man, S. Chen, X. Li, *Corros. Sci., 118(2017)31*
29. Z. Cui, S. Chen, Y. Dou, S. Han, L. Wang, C. Man, X. Li, *Corros Sci*.,150(2019)218
30. F. Di Quarto, S., Piazza, & C. Sunseri, *Corros. Sci., 31(1990)721*

31. Z. Feng, X. Cheng, C. Dong, L. Xu, & X. Li, *Corros. Sci., 52(2010)3646*
32. J.-B. Lee, & S.-I. Yoon, *Mater. Chem. Phys., 122(2010)194*
33. Y. Cui, M. S. Qurashi, J. Wang, T. Chen, J. Bai, N. Dong, P. Han, *Steel Res Int., (2019)*
34. C. O'Laoire, B. Timmins, L., Kremer, J. D. Holmes, & M. A. Morris, *Anal. Lett., 39(2006)2255*
35. S. Zhang., H. Li., Z. Jiang., B. Zhang., Z. Li., J. Wu., S. Fan., H. Feng., H. Zhu., *Mater. Charact., 152(2019)141*
36. J.F. Moulder, W.F. Stickle, P.E. Sobol, K.D. Bomben, Handbook of X-ray Photoelectron Spectroscopy, Perkin–Elmer, Physical Electronic Division, Eden Praire, MN, (1992).
37. C. Loable, I. N. Viçosa, T. J. Mesquita, M. Mantel, R. P. Nogueira, G. Berthomé, V. Roche, *Mater. Chem. Phys.,* 186(2017)237
38. P. Pistorius, & M. Du Toit, Low-nickel austenitic stainless steels: Metallurgical constraints. Proceedings of the 12th International Ferroalloys Congress: Sustainable Future. (2010). 911-917.
39. V. Maurice, H. Peng, L. H. Klein, A. Seyeux, S. Zanna, & P. Marcus, *Faraday Discuss.,* 180(2015)151